Strain Shielding for Cemented Hip Implants

Yekutiel Katz[a], Zohar Yosibash[a], Moshe Salai[b], Nimrod Snir[b]

[a]*School of Mechanical Engineering, The Iby and Aladar Fleischman Faculty of Engineering, Tel-Aviv University, Ramat-Aviv, Israel*
[b]*Division of Orthopaedic Surgery, Tel Aviv Sourasky Medical Center, Sackler Faculty of Medicine, Tel Aviv University, Tel Aviv, Israel.*

Abstract

Background: Long-term survival of hip implants is of increasing relevance due to the rising life expectancy. The biomechanical effect of strain shielding as a result of the implant insertion may lead to bone resorption, thus increase risk for implant loosening and periprosthetic fractures. Patient-specific quantification of strain shielding could assist orthopedic surgeons in choosing the biomechanically most appropriate prosthesis.

Methods: Validated quantitative CT-based finite element models of five femurs in intact and implanted states were considered to propose a systematic algorithm for strain shielding quantification. Three different strain measures were investigated and the most appropriate measure for strain shielding quantification is recommended. It is used to demonstrate a practical femur-specific implant selection among three common designs.

Findings: Strain shielding measures demonstrated similar trends in all Gruen zones except zone 1, where the volumetric strain measure differed from von-Mises and maximum principal strains. The volumetric strain measure is in better agreement with clinical bone resorption records. It is also consistent with the biological mechanism of bone remodeling so it is recommended for strain shielding quantification. Applying the strain shielding algorithm with three different implants for a specific femur suggests that the collar design implant is preferable. Such quantitative biomechanical input is valuable for practical patient specific implant selection.

Interpretation: Volumetric strain should be considered for strain shielding examination. The presented methodology may potentially enable patient-specific pre-operative strain shielding evaluation so to minimize strain shielding. It should be further used in a longitu-

Email address: yosibash@tauex.tau.ac.il (Zohar Yosibash)

dinal study so to correlate between strain shielding predictions and clinical bone resorption.

Keywords:
Hip prosthesis, strain shielding, finite element analysis

1. Introduction

Total hip replacements (THRs) are a common procedure (Pabinger and Geissler, 2014; Kurtz et al., 2007) with a revision rate of 6.45% after five years and 12.9% after ten years (Labek et al., 2011). Almost half of patients are expected to undergo a revision surgery within 25 years (Evans et al., 2019). Long-term THR survivorship is of increasing relevance due to the rising life expectancy, thus, investigation of the biomechanical prosthesis-femur response is of interest.

Cemented femoral prostheses are implanted in the majority of THRs in several countries (Swedish Hip Arthroplasty Register, 2018; National Joint Registry for England, Wales, Northern Ireland and the Isle of Man, 2018; The New Zeland Joint Rregistry, 2019). The cemented stems are frequently reported to have a better clinical outcome compared to cementless stems (Yang et al., 2019; Lin et al., 2019; Mäkelä et al., 2014; Veldman et al., 2017; Barenius et al., 2018; Abdulkarim et al., 2013). The uniformly distributed cement mantle forms a mechanical interlock between the bone and the stem enabling an even and gradual load transfer (Kuehn et al., 2005).

Inserting a metallic prosthesis into a femur changes the state of stress and strains in bone's tissue, leading to a decrease in bone mineral density (BMD) due to "stress shielding" or better termed "strain shielding". BMD changes reduce implants' mechanical stability, thus increasing the risk for aseptic loosening (Sundfeldt et al., 2006). Bone strength is also decreased, thus increasing the risk for periprosthetic fracture. The combined factors are the cause for 60% of THR revisions (Sadoghi et al., 2013; Ulrich et al., 2008).

Bone remodeling is governed by mechanical stimuli (Klein-Nulend et al., 2013), thus it is conceivable that post-operative strain shielding affects implant's long term biomechanical performance. Quantification of the strain shielding may assist surgeons in choosing the most appropriate patient specific implant, especially in view of the new 3D printing technologies.

Strain shielding can be quantified using finite element analyses (FEA), that allow to determine strains within intact and implanted femurs under physiological loading conditions (Trabelsi et al., 2011; Bessho et al., 2007; Schileo et al., 2014; Rohlmann et al., 1983; Pettersen et al., 2009; Yosibash et al., 2012; Katz et al., 2018). In the current study, quantitative-CT (QCT) based finite element (FE) models of five femurs, both males and females, at different ages and in intact and implanted states (different prostheses) were considered. These models were experimentally validated in previous studies (Katz et al., 2018; Katz and Yosibash, 2020) and in Appendix A (accounting both for femoral and implant strains) and are used here to determine strain shielding.

A quantitative assessment of strain shielding depends on: (a) the loading conditions, (b) the regions in the femur which the strain shielding is computed, (c) the type of strains considered (strain measures, i.e. equivalent von-Mises strain, principal max strain, etc).

A variety of "physiologic-like" loading conditions are documented in past literature. Some are simple, considering hip contact force alone (Goshulak et al., 2016), some include the abductor muscles (Pettersen et al., 2009; Hirata et al., 2013) and some consider multiple muscles (Abdullah et al., 2010; Yamako et al., 2014; Moussa et al., 2017; Szwedowski et al., 2012; Cilla et al., 2017). Since the femoral head is replaced by a prosthesis, it is conceivable that the hip contact force is the load that has the largest influence on strain variations in the bone tissue. Thus, the hip contact force is the loading considered for quantifying the strain shielding in the different regions in the femur.

In many previous studies only bone's surfaces (Pettersen et al., 2009; Abdullah et al., 2010) or prosthesis surfaces (Yamako et al., 2014; Moussa et al., 2017) were examined rather than the bone tissue inside the femur. Drawing quantitative conclusions based only on the bone-prosthesis interface is problematic because of bone-implant contact assumptions. Relaying on the femur's outer surface alone is also limited since bone remodeling is manifested in the inner bone tissue. Thus, considering femur's inner tissue for strain shielding assessment should be the proper choice.

Change in strain distribution in the bone tissue, i.e. the difference between the strain field before and after the prosthesis is inserted, was rarely quantified and mostly qualitatively

discussed in past studies. In the few studies where this difference was quantified, a relative difference was commonly used (Pettersen et al., 2009; Goshulak et al., 2016). Such an approach may be misleading because in areas where strains are small, a small change will cause a large relative difference, predicting high bone resorption. We adopt here the procedure in (Cilla et al., 2017), and consider an absolute value of strain change for quantification of strain shielding.

The appropriate strain measure to evaluate strain shielding remains an open question. A variety of strain and stress measures were considered, based on: von Mises stress (Hirata et al., 2013; Yamako et al., 2014; Matsuyama et al., 2016; Moussa et al., 2017), von Mises strain (Pettersen et al., 2009; Szwedowski et al., 2012), Tresca stress (Abdullah et al., 2010), strain energy density (Yamako et al., 2014; Szwedowski et al., 2012), principal strains (Cilla et al., 2017) and principal stresses (Abdullah et al., 2010). Because the biological mechanosensation mechanism is strain-driven (Klein-Nulend et al., 2013; Liu et al., 2010; Weinbaum et al., 1994) we concentrate on strain related measures.

The aim of the current work is to: (a) Propose an algorithm for strain shielding quantification following the insertion of cemented hip implants. (b) Examine if strain shielding depends on the selected strain measure. (c) Examine if the adopted strain shielding may explain clinical data available in past publications (BMD changes following THR).

By using the recommended strain shielding measure the surgeon may quantify, among available prostheses, which one minimizes the shielding. Such an analysis is demonstrated by investigating the strain shielding among three common designs: regular, high offset and collar .

The presented methodology has the potential to be incorporated in clinical practice and in longitudinal studies to correlate predicted strain shielding with clinical outcome.

2. Methods

2.1. Femurs and Prostheses

Five fresh frozen femurs from four donors (male and female at various ages) and five different cemented hip prostheses were considered. A summary of donors and prostheses is

provided in Table 1 and shown in Figure 1. All femurs were QCT-scanned in their intact condition and after prosthesis insertion.

Patient specific QCT-based FE models were constructed for each of the femurs in intact and implanted states. These models were validated by experiments under stance loading conditions in Katz et al. (2018); Katz and Yosibash (2020) and in Appendix A (that details the experiments performed on FFI1R).

Briefly, the intact femurs were loaded in stance position by applying a hip contact force to their head at various angles. The femurs were thereafter implanted with different cemented prostheses by an orthopedic surgeon and re-tested. On all femurs and prostheses strain gauges were bonded to monitor the strains during loading (FFI1R was monitored using digital image correlation). The measurements were used to validate the FE models which are used herein.

Table 1: Donors and prostheses details.

		Donor						Prosthesis	
		Gender	Age (y)	Height (cm)	Weight (kg)	Side	Death cause	Manufacturer	Model
(a)	FFM7R	Female	75	162	41	R	cervical cancer	Protec	LOT 2018 7.5 mm
(b)	FFB1R	Male	67	178	84	R	heart failure	Protec	LOT 2132 10 mm
(c)	FFB1L					L		Groupe Lepine	PAV ® H015 0214
(d)	FFY	Male	20	185	68	L	drug overdose	Aesculap	ISONIC NK 082 s8
(e)	FFI1R	Female	80	168	97	R	heart disease	DePuy Synthes	CORAIL® polished 11

2.2. Finite element analyses (FEAs)

Strains in the bone are investigated by using high-order linear FE analyses (Szabo and Babuska, 1991) of the intact and implanted femurs. FE models of all bones were generated based on QCT scans, and were shown to well predict the strains on femurs' and prostheses' surfaces (Katz and Yosibash, 2020; Katz et al., 2018; Yosibash et al., 2012).

FE models of implanted femurs were generated by virtually inserting the prosthesis into the intact femur while mimicking it's actual position, determined by CT scans and X-rays of the implanted femurs. The prostheses models were constructed from 3D scans of the actual implants.

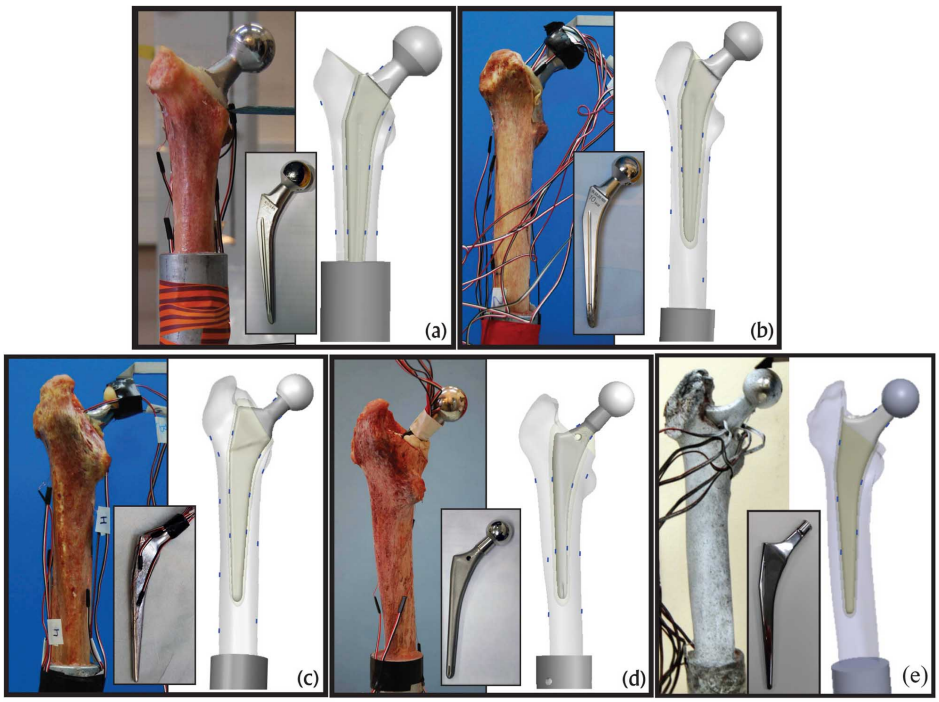

Figure 1: The five femurs and prostheses (blue points denote location of strain gauges). (a) FFM7R (b) FFB1R (c) FFB1L (d) FFY (e)FFI1R. Images (a)-(d) are from Katz et al. (2018).

The contact conditions between bone and implant as well as the cement thickness and distribution cannot be defined accurately from QCT scans or X-ray radiographs. A perfect bonding condition was applied on bone implant interface (cement thickness was shown to have minor influence on cortical bone strains in Katz et al. (2018), thus it was set to zero).

Because only the femoral head is replaced, we choose to apply only the hip contact force in our experimants and FEA to asses the difference between the intact and implanted states. Loading directions of 0^o and 7^o were considered, as also used in the FE validation studies (Katz et al., 2018). In the FEAs the location and direction of the simulated force was kept identical in both intact and implanted models so that the moment acting on the intact and implanted femurs is the same. FE calculated femoral strains were extracted at the plane of prosthesis symmetry (midplane). Three different strain measures on the midplane were considered for strain shielding quantification:

- von-Mises strain (equivalent strain) - commonly used for bones in the literature (Pet-

tersen et al., 2009).

$$\varepsilon_{vM} = \sqrt{\frac{(\varepsilon_1 - \varepsilon_2)^2 + (\varepsilon_2 - \varepsilon_3)^2 + (\varepsilon_3 - \varepsilon_1)^2}{2}} \tag{1}$$

- Volumetric strain (trace($\boldsymbol{\varepsilon}$)). This measure is considered because bone remodelling is pressure related. Biological load sensing mechanism is attributed to volumetric strain (Henstock et al., 2013):

$$\varepsilon_t = \varepsilon_1 + \varepsilon_2 + \varepsilon_3 \tag{2}$$

- Maximum principal strain - commonly used in bones as a failure criterion (Schileo et al., 2008a; Yosibash et al., 2010).

$$\varepsilon_{mp} = max(\varepsilon_1, |\varepsilon_3|) \tag{3}$$

where $\boldsymbol{\varepsilon}_1, \boldsymbol{\varepsilon}_2, \boldsymbol{\varepsilon}_3$ are the principal strains.

To allow a comparison between the different femurs, belonging to donors of different body weights, we normalize the strains in the FEA by considering a hip contact force equal to donor's weight.

2.3. Quantification of strain shielding

The intersection of the prosthesis midplane and the femur is divided into seven zones similar to the clinical Gruen zones (Gruen et al., 1979) as illustrated in Figure 2(c). The zones are defined as follows: zones 1 and 7 are above lesser trochanter, zone 1 being the greater trochanter and zone 7 being the calcar region. Zones 2,3 (laterally) and 5,6 (medially) are of equal length and are separated at the middle between the lesser trochanter and tip of the prosthesis. Zone 4 starts at the tip of the prosthesis and ends distally at a distance of 15mm. Most zones are in the femoral shaft, where the cortical bone dominates the mechanical response. The trabecular bone is removed during the implantation procedure (by broaching or reaming) and the gap between the prosthesis and the cortex is filled with cement. Thus, in zones 2-7 only the cortical cross-section area is considered (defined as the area in which ρ_{ash}>0.7 [gr/cc] (Schileo et al., 2008b)). In zone 1 (greater trochanter) where very little

cortex is found, a small offset of ~3mm from the prosthesis is dismissed, this gap represents the cement (Isaac et al., 2000) and is thus irrelevant for strain shielding evaluation. In each zone i the average strain difference ϵ_j^i is computed, defined by:

$$\epsilon_j^i = \frac{\iint_{\Omega_i} \varepsilon_j^{implanted} - \varepsilon_j^{intact} d\Omega_i}{\Omega_i} \tag{4}$$

where j is either vM, t or mp and Ω_i (i=1 to 7) are the various Gruen zones i.e. ϵ_j^i is the strain shielding measure i in Gruen zone j. Negative ϵ indicates reduced strains predicting bone resorption, while positive ϵ is an indication of increased strains. The methodology for the computation of the different ϵ_j^is is illustrated in Figure 2.

Strains computed in intact and implanted models (at the implant's midplane) were considered in the same location if the distance between the corresponding points was below 0.5mm. The resulting pointwise difference of each of the strain measures is illustrated in Figure 2(c). These were computed for the five femurs, each implanted by a different prosthesis. The average difference over each Gruen zone was considered.

To allow comparison between the three examined measures so to determine which is the most indicative for clinical use. The strain shielding obtained in each Gruen zone was presented as percentage of the strain shielding in Gruen zone 7 (where strain shielding is mostly pronounced).

2.4. Selection of an "optimal" implant

To demonstrate the use of the quantitative strain shielding for a specific patient we chose FFI1R as an example. FFI1R was implanted with the CORAIL® prosthesis (DePuy Synthes, Raynham, MA, USA) which has several design variations. To investigate the induced strain shielding, three different designs of the CORAIL® prosthesis were examined: polished 'standard', polished 'high offset' and a polished 'collared' design that was virtually constructed based on the cementless design. These were virtually implanted in the FE model of FFI1R. Strain shielding was computed and compared between the three prostheses.

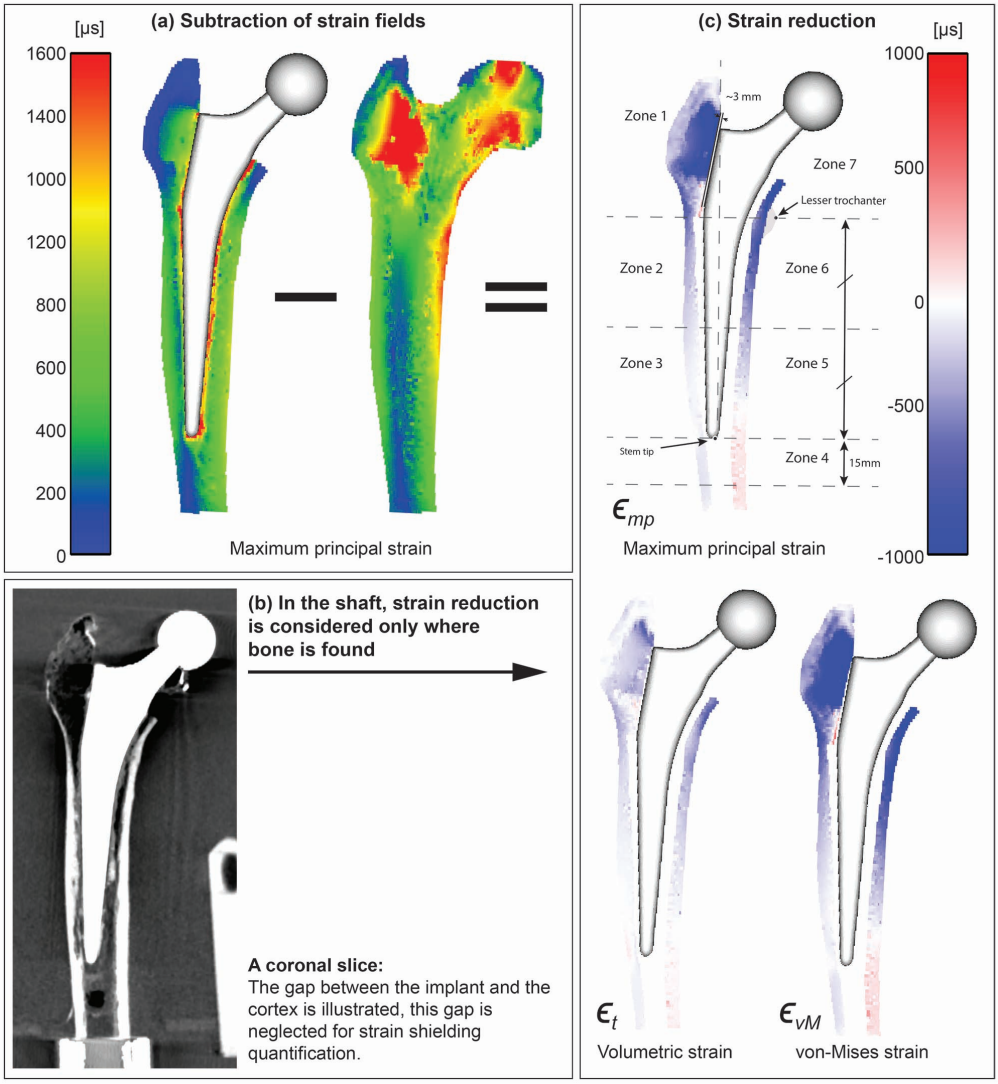

Figure 2: Strain shielding quantification algorithm. (a) Subtraction of the strain field obtained at prosthesis midplane. (b) Illustration of the gap found between bone and prosthesis at the shaft. At the shaft, only areas containing cortical bone are considered. (c) The obtained strain reduction fields, three measures are examined. These fields may be further divided and averaged over the illustrated Gruen zones.

3. Results

3.1. Strain shielding measures

The three strain shielding measures (ϵ_{vM}, ϵ_{mp} and ϵ_t), in the seven Gruen zones under two hip contact force directions were computed for all femurs. For example, Figure 3 illustrates the change in the volumetric strain. One may observe that different femurs have different

cortical areas for strain shielding assessment: for example, zones 7,6 and 5 in FFM7R are much smaller compared to the other femurs.

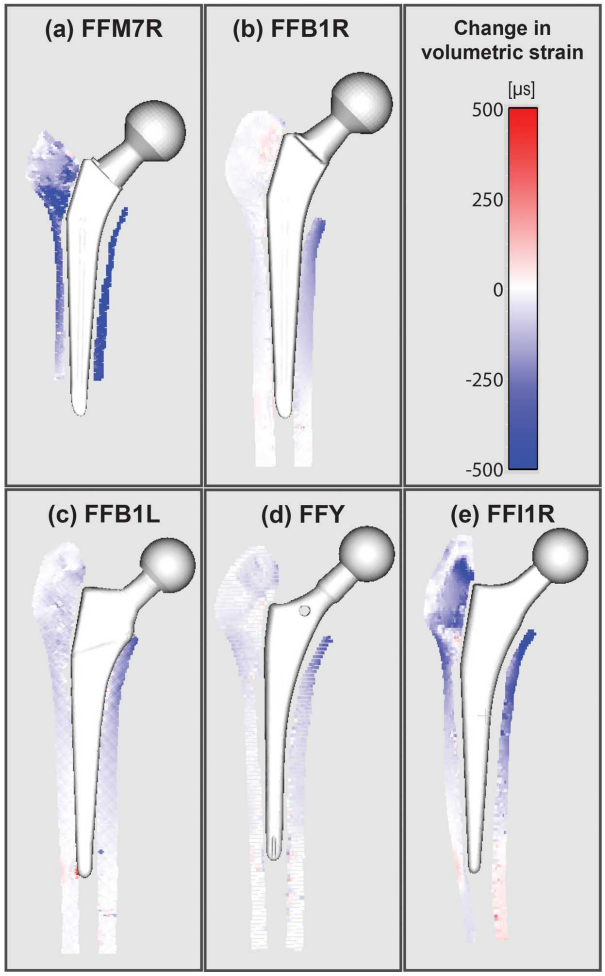

Figure 3: Volumetric strain reduction for the five examined femurs (7^o angle considered).

Histograms presenting strain shielding percentage relative to zone 7 are shown in Figure 4. In Gruen zones 2-6, all strain shielding measures show similar reduction in all femurs under both loading conditions. Zone 1 (greater trochanter) is exceptional in which the strain shielding measures disagree. The general trend suggests that von-Mises and principal strain measures similarly predict a rise in strain shielding compared to zone 2. The volumetric strain however, predicts lower values which are similar or below the values in zone 2. A slightly more pronounced strain shielding was found at 0^o loading than at 7^o in all zones. Zone 7 (calcar region) experienced the most pronounced strain shielding in all cases.

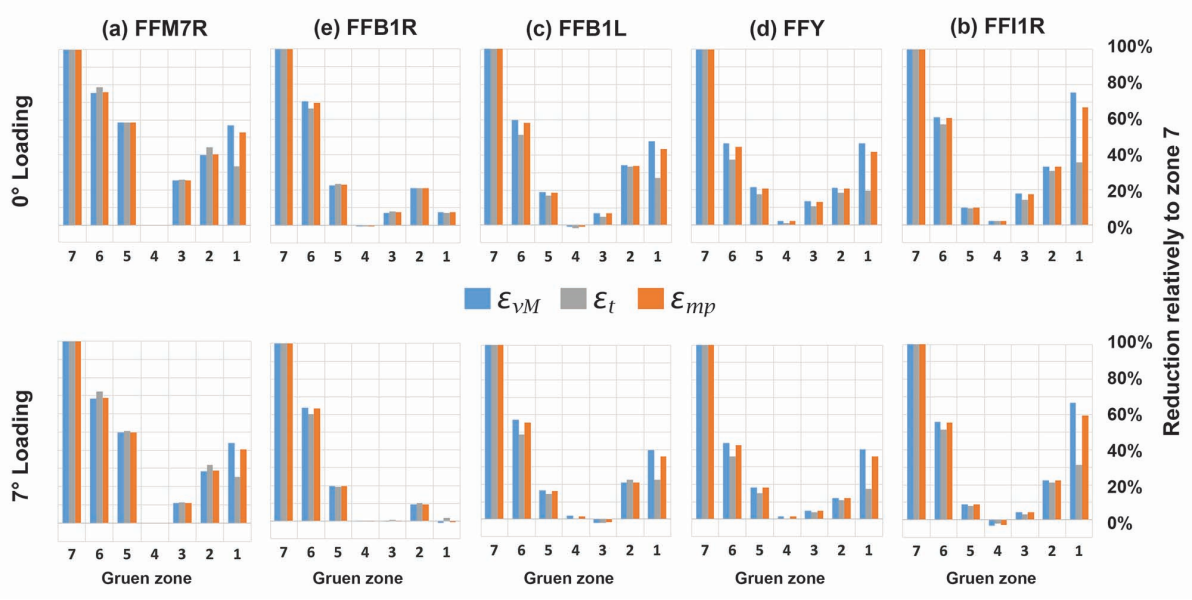

Figure 4: Strain shielding in Gruen zones (absolute difference) relatively to zone 7. Different strain shielding measures examined.

A general pattern in strain shielding relative to zone 7 can be observed regardless of the examined strain measure and considering both loading angles in zones 2-6: zone 2: <35% (22±8%); zone 3: <18% (6±6%); zone 4: <2% (0±2%); zone 5: <23% (16±5%); zone 6: <70% (55±9%). In zone 1 the strain measures disagree, ϵ_{vM} and ϵ_{mp} predicted values of <75% (38±23%) while ϵ_t resulted in lower predictions of <48% (20±11%).

We exclude FFM7R where the prosthesis penetrated the imbedding cylinder (see Figure 1) causing additional constraint on the prosthesis by covering its distal end. FFM7R is provided only to examine the difference between the different strain shielding measures. However, it cannot be used to derive the typical strain shielding pattern relatively to zone 7. It does not represent stain shielding in a typical femur.

3.2. Examination of different prostheses for a specific femur

FE simulations of the intact FFI1R and after different prosthesis insertion are illustrated in Figure 5. Strains reduction relatively to the intact state is evident. The collared prosthesis induces high strains at the calcar region compared to other prostheses. The high offset design increases strains distally.

Choosing the strain shielding measure as the volumetric strain, we computed the strain shielding for the three prostheses implanted virtually in FFI1R (Figure 6). The hip contact force is applied to the femur and prosthesis at 7^o.

Comparing to the "regular prosthesis", the collared prosthesis affects only Gruen zone 7 reducing strain shielding by 20%. The high offset prosthesis affects all zones by reducing strain shielding. In zones 3,4,5 strains are increased rather than shielded. In zones 2 and 6 strain shielding was reduced by 37% and 21% respectively. Zone 7 however, is least affected (3%).

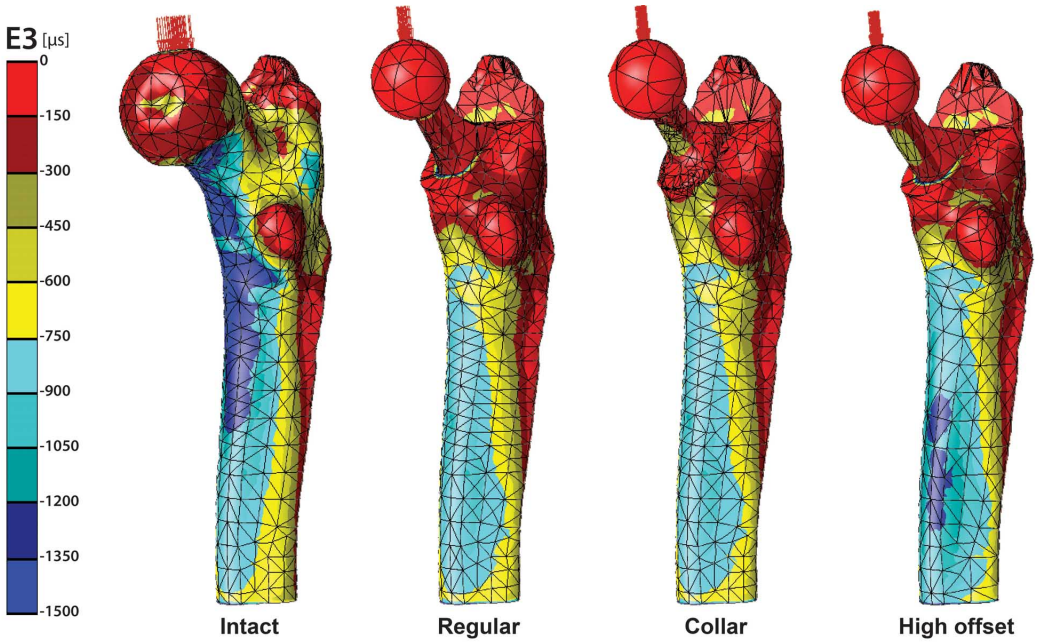

Figure 5: FFI1R simulated in an intact state and with the three examined prostheses.

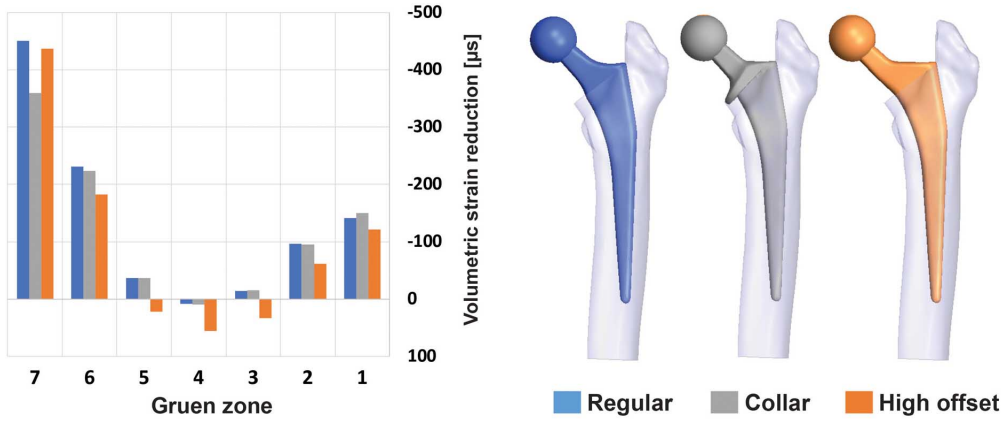

Figure 6: Strain shielding based on volumetric strain (ϵ_t) for the three CORAIL prostheses implanted in FFI1R FE model and loaded at 7^o.

4. Discussion

A systematic algorithm for strain shielding quantification has been presented. It aims to enable pre-operative evaluation of strain shielding so to match the most appropriate implant for a specific patient. Such a methodology may assist in improving implant designs as well as in designing patient specific implants by additive manufacturing.

First, we demonstrated that FEA of five femurs with five different implants represents well the experimental observations (in Katz et al. (2018), Katz and Yosibash (2020) and Appendix A), and may be reliably used to quantify strain shielding. This is essential since strains within the bone tissue cannot be measured but only computed. Strain shielding was quantified using different strain measures, resulting in similar strain reduction patterns in all Gruen zones with the exception of zone 1 where the volumetric measure differed from the von-Mises and the max-principal strain measures.

4.1. Comparison of different strain measures

Principal maximum (ϵ_{mp}) and von-Mises strain (ϵ_{vM}) measures predicted similar strain shielding patterns. The volumetric strain measure ϵ_t was different, mostly in Gruen zone 1. According to the results presented in Figure 4, in all examined femurs (with the single exception of FFB1R where no difference was found between the strain measures), ϵ_{mp} and

ϵ_{vM} measures imply that strain shielding is more pronounced proximally i.e. Gruen zone 1 experiences high strain shielding, particulary higher than zone 2. The volumetric strain ϵ_t however, suggests that zone 1 experiences strain shielding rates lower than or similar to zone 2.

The strain shielding pattern based on ϵ_t is in a better agreement with clinical bone resorption records. Several studies documented BMD changes in patients following a cemented hip replacement (Jayasuriya et al. (2013); Li et al. (2007); Venesmaa et al. (2003); Digas and Karrholm (2008); Buckland et al. (2010); Bieger et al. (2011); Knutsen et al. (2017)). These are based on dual-energy X-ray absorptiometry (DEXA) and also refer to Gruen zones which are common and familiar to the clinical community. All studies report a similar trend - the least bone resorption usually occurs around the tip of the prosthesis at zones 3,4,5 followed by zones 2,6. Largest reduction in BMD is found in zone 7. This trend is well captured by the methodology suggested herein regardless of the strain measure considered. In zone 1, the clinical studies report strain shielding rates below or similar to zone 2 (with the single exception of (Buckland et al., 2010) who examined a similar implant as (Jayasuriya et al., 2013) resulted in contradicting findings in zone 1). Based on clinical observations of BMD reduction we propose the volumetric strain as the appropriate strain measure for strain shielding quantification. Additionally, the use of volumetric strain for strain shielding evaluation is consistent with the biological mechanism attributed to bone remodeling, shown to be regulated by hydrostatic pressure (Klein-Nulend et al., 2013; Liu et al., 2010; Henstock et al., 2013; Scheiner et al., 2016; Pastrama et al., 2018). To the best of our knowledge, no previous study considered volumetric strain measure for strain shielding assessment.

Comparing the strain shielding patterns obtained at 0^o and 7^o loading, no significant difference is observed. The relative strain shielding is slightly more pronounced at 0^o loading than at 7^o. At 0^o the moment acting on the femur is larger, leading to larger strains. This effect is more pronounced in the intact femur leading to larger strain reduction in comparison to the implanted configuration, i.e. causing a more pronounced strain shielding. The overall trend, however, does not change. Thus among the examined stance position loadings, a single direction at 7^o may be sufficient for strain shielding assessment.

4.2. Choosing an "optimal" implant

To demonstrate a potential preoperative use of the presented algorithm, we examined the strain shielding based on volumetric strain (ϵ_t) induced by three common prostheses on the same femur. All prosthesis were of the same size, referred to as "regular", "high-offset" and "collar". The "collar" polished design was virtually constructed since in reality it is cementless and nonpolished.

The "collar" affects only Gruen zone 7 (reducing strain shielding by 20%) while other zones are unaffected. The high offset prosthesis increases the moment acting on the femur thus increasing the strains. Consequently, strain shielding is reduced in all zones. Zone 7 however, where strain shielding is mostly pronounced, is leased affected, experiencing the least reduction in strain shielding (3%). Additionally, an increase in strain is obtained distally in the zones around the prosthesis tip (zones 3-5) which may increase the risk of periprosthetic fractures (type B2 and C periprosthetic fractures defined in Schwarzkopf et al. (2013)). Despite the positive influence on zones 2 and 6 (strain shielding reduced by 37% and 21% respectively), the overall effect of the high offset implant is mostly negative. Thus, the collar design may be preferable for the examined femur when considering biomechanical effects.

4.3. Correlating strain shielding with clinically observed BMD reduction

It is conceivable that post operative strain shielding assessment is correlated with long term BMD changes however, it has yet to be proven. Only limited evidence is found in the literature on the correlation between FE based BMD reduction predictions and clinical observations. A study performed by (Hirata et al., 2013) found a correlation between the simulated postoperative 'equivalent stress' to bone mineral density (BMD) change in zone 7 (20 patients). A low coefficient of determination was reported (r^2=0.27). A stress measure was computed and only FE models of implanted femurs were considered. No comparison to the intact state of the bone was performed. These modifications may improve the correlation and reveal additional correlations examining other Gruen zones. Another study by (Szwedowski et al., 2012) considered different algorithms for remodeling using FE methods compared to clinical observations of BMD change (3 patients). Bone remodelling algorithms

aim at predicting long term outcome based on the post-operative conditions. A long term outcome involves time-dependent modeling assumptions as well as bone prosthesis contact conditions that make these predictions questionable. To the best of our judgement only postoperative mechanical conditions (relatively to the intact state) may be used to correlate with patient specific long term outcome. The aforementioned studies (Hirata et al., 2013; Szwedowski et al., 2012) are among the few that addressed clinical observations to validate their BMD predictions (both considered cementless prostheses).

4.4. Limitations and future work

The strain shielding algorithm may be used in a longitudinal study to correlate between predictions and bone resorption. A pre-operative CT scan must be available to allow the creation of a patient specific FE model of the intact and implanted femur. Such a patient must then be monitored for BMD changes at the Gruen zones. The BMD changes are to be compared to the pre-operatively predicted strain shielding to examine correlation in each Gruen zone separately. Such a study is a prospective long term one that must be performed in the future.

Additionally, more loading configurations simulating activities such as for example stair climbing, should also be examined.

It is also important to study wether different prostheses are more appropriate for different patients, or does there exist a unique design that is optimal for majority of patients. Using the suggested methodology, a comparison of different prostheses for same patient, or different patients with same prosthesis may be of financial significance for clinical centers.

In our study we assumed that the surgeon does not deviate from the planed position of the prosthesis. The robustness of prosthesis' performance to small deviations in orientation will be studied in the future.

Conflict of Interest

YK, NS, MS have no conflicts of interest to declare. ZY has a financial interest in PerSimiO.

References

C. Pabinger, A. Geissler, Utilization rates of hip arthroplasty in OECD countries, Osteoarthritis Cartilage 22 (6) (2014) 734–741.

S. Kurtz, K. Ong, E. L. F. Mowat, M. Halpern, Projections of primary and revision hip and knee arthroplasty in the United States from 2005 to 2030., J. Bone Joint Surg. Am. 89A (4) (2007) 780–785.

G. Labek, M. Thaler, W. Janda, M. Agreiter, B. Stockl, Revision rates after total joint replacement: cumulative results from worldwide joint register datasets, J. Bone Joint Surg. Br. 93B (7) (2011) 293–297.

J. T. Evans, J. P. Evans, R. W. Walker, A. W. Blom, M. R. Whitehouse, A. Sayers, How long does a hip replacement last? A systematic review and meta-analysis of case series and national registry reports with more than 15 years of follow-up, Lancet 393 (2019) 647–654.

Swedish Hip Arthroplasty Register, Annual Report 2017, URL `https://registercentrum.blob.core.windows.net/refdocs/10.18158/BJxLUfemL4.pdf`, 2018.

National Joint Registry for England, Wales, Northern Ireland and the Isle of Man, 15th Annual Report, URL `https://www.hqip.org.uk/wp-content/uploads/2018/11/NJR-15th-Annual-Report-2018.pdf`, 2018.

The New Zeland Joint Rregistry, Twenty year report january 1999 to december 2018, URL `https://nzoa.org.nz/system/files/DH8328_NZJR_2019_Report_v4_7Nov19.pdf`, 2019.

C. Yang, X. Han, J. Wang, Z. Yuan, T. Wang, M. Zhao, G. Han, Cemented versus uncemented femoral component total hip arthroplasty in elderly patients with primary osteoporosis: retrospective analysis with 5-year follow-up, J. Int. Med. Res. 47 (4) (2019) 11610–19.

F. F. Lin, Y. F. Chen, B. Chen, C. H. Lin, K. Zheng, Cemented versus uncemented hemiarthroplasty for displaced femoral neck fractures: A meta-analysis of randomized controlled trails, Medicine 98 (8) (2019) e14634.

K. T. Mäkelä, M. Matilainen, P. Pulkkinen, A. M. Fenstad, L. Havelin, L. Engesaeter, O. Furnes, A. B. Pedersen, S. Overgaard, J. Kärrholm, H. Malchau, G. Garellick, J. Ranstam, A. Eskelinen, Failure rate of cemented and uncemented total hip database of four nations, BMJ 348 (2014) f7592.

H. D. Veldman, I. C. Heyligers, B. Grimm, T. A. Boymans, Cemented versus cementless hemiarthroplasty for a displaced fracture of the femoral neck: a systematic review and meta-analysis of current generation hip stems., Bone Joint J. 99-B (4) (2017) 421–431.

B. Barenius, C. Inngul, Z. Alagic, A. Enocson, A randomized controlled trial of cemented versus cementless arthroplasty in patients with a displaced femoral neck fracture: a four-year follow-up., Bone Joint J. 100-B (8) (2018) 1087–93.

A. Abdulkarim, P. Ellanti, N. Motterlini, T. Fahey, J. M. O'Byrne, Cemented versus uncemented fixation in total hip replacement: a systematic review and meta-analysis of randomized controlled trials., Orthop. Rev. 5 (1) (2013) 34–44.

K. D. Kuehn, W. Ege, U. Gopp, Acrylic bone cements: composition and properties, Orthop. Clin. N. Am. 36 (2005) 17–28.

M. Sundfeldt, L. V. Carlsson, C. B. Johansson, P. Thomsen, C. Gretzer, Aseptic loosening, not only a question of wear. A review of different theories, Acta Orthop. 77 (2) (2006) 177–197.

P. Sadoghi, M. Liebensteiner, M. Agreiter, A. Leithner, N. Bohler, G. Labek, Revision Surgery After Total Joint Arthroplasty: A Complication-Based Analysis Using Worldwide Arthroplasty Registers, J. Arthroplasty 28 (8) (2013) 1329–32.

S. D. Ulrich, T. M. Seyler, D. Bennett, R. E. Delanois, K. J. Saleh, M. Thongtrangan, I.and Kuskowski, E. Y. Cheng, P. F. Sharkey, J. Parvizi, J. B. Stiehl, M. A. Mont, Total hip arthroplasties: What are the reasons for revision?, Int. Orthop. 32 (5) (2008) 597–604.

J. Klein-Nulend, A. D. Bakker, R. G. Bacabac, A. Vatsa, S. Weinbaum, Mechanosensation and transduction in osteocytes, Bone 54 (2) (2013) 182–190.

N. Trabelsi, Z. Yosibash, C. Wutte, R. Augat, S. Eberle, Patient-specific finite element analysis of the human femur - a double-blinded biomechanical validation, J. Biomech. 44 (2011) 1666 – 1672.

M. Bessho, I. Ohnishi, J. Matsuyama, T. Matsumoto, K. Imai, K. Nakamura, Prediction of strength and strain of the proximal femur by a CT-based finite element method, J. Biomech. 40 (8) (2007) 1745–1753.

E. Schileo, L. Balistreri, L. Grassi, L. Cristofolini, F. Taddei, T. Medica, I. O. Rizzoli, To what extent can linear finite element models of human femora predict failure under stance and fall loading configurations?, J. Biomech. 47 (14) (2014) 3531–3538.

A. Rohlmann, U. Mossner, G. Bergmann, R. Kolbel, Finite-Element-Analysis And Experimental Investigation In A Femur With Hip Endoprosthesis, J. Biomech. 16 (9) (1983) 727–742.

S. H. Pettersen, T. S. Wik, B. Skallerud, Subject specific finite element analysis of stress shielding around a cementless femoral stem, Clin. Biomech. 24 (2009) 196–202, 1st Corrigendum, Clin. Biomech., 24(8), 2009, p. 697. 2nd Corrigendum, Clin. Biomech., 26(4), 2011, p. 429.

Z. Yosibash, A. Katz, C. Milgrom, Toward verified and validated FE simulations of a femur with a cemented hip prosthesis, Med. Eng. Phys. 35 (7) (2012) 978–987.

Y. Katz, O. Lubovsky, Z. Yosibash, Patient-specific finite element analysis of femurs with cemented hip implants, Clin. Biomech. 58 (2018) 74–89.

Y. Katz, Z. Yosibash, New insights on the proximal femur biomechanics using Digital Image Correlation, J. Biomech. 101 (2020) 109599.

P. Goshulak, S. Samiezadeh, M. S. R. Aziz, H. Bougherara, R. Zdero, E. H. Schemitsch, The biomechanical effect of anteversion and modular neck offset on stress shielding for short-stem versus conventional long-stem hip implants, Med. Eng. Phys. 38 (2016) 232–240.

Y. Hirata, Y. Inaba, N. Kobayashi, H. Ike, H. Fujimaki, T. Saito, Comparison of mechanical stress and change in bone mineral density between two types of femoral implant using finite element analysis, J. Arthroplasty 28 (10) (2013) 1731–5.

A. H. Abdullah, M. N. M. Asri, M. S. Alias, T. Giha, Finite Element Analysis of Cemented Hip Arthroplasty: Influence of Stem Tapers, Lecture Notes in Engineering and Computer Science: Proceedings of The International Multi Conference of Engineers and Computer Scientists. IMECS 2010, 17-19 March, 2010, Hong Kong (2010) 2241–46.

G. Yamako, E. Chosa, X. Zhao, K. Totoribe, S. Watanabe, T. Sakamoto, N. Nakane, Load-transfer analysis after insertion of cementless anatomical femoral stem using pre- and post-operative CT images based patient-specific finite element analysis, Med. Eng. Phys. 36 (2014) 694–700.

A. A. Moussa, J. Fischer, R. Yadav, M. Khandaker, Minimizing stress shielding and cement damage in cemented femoral component of a hip prosthesis through computational design optimization, Adv. Orthop. (2017) 8437956.

T. D. Szwedowski, W. R. Taylor, M. O. Heller, C. Perka, M. Muller, G. N. Duda, Generic rules of mechano-regulation combined with subject specific loading conditions can explain bone adaptation after THA, PLoS ONE 7 (5).

M. Cilla, S. Checa, G. Duda, Strain shielding inspired re-design of proximal femoral stems for total hip arthroplasty, J. Orthop. Res. 35 (2017) 2534–2544.

K. Matsuyama, Y. Ishidou, Y. M. Guo, H. Kakoi, T. Setoguchi, S. Nagano, I. Kawamura, S. Maeda, S. Komiya, Finite element analysis of cementless femoral stems based on mid- and long-term radiological evaluation, BMC Musculoskelet. Disord. 17 (1) (2016) 397.

C. Liu, Y. Zhao, W. Y. Cheung, R. Gandhi, L. Wang, L. You, Effects of cyclic hydraulic pressure on osteocytes, Bone 46 (2010) 1449–1456.

S. Weinbaum, S. C. Cowin, Y. Zeng, A model for the excitation of osteocytes by mechanical loading-induced bone fluid shear stresses, J. Biomech. 27 (3) (1994) 339–360.

B. Szabo, I. Babuska, Finite Element Analysis, pub-JW, New York, 1991.

J. R. Henstock, M. Rotherham, J. B. Rose, A. J. El Haj, Cyclic hydrostatic pressure stimulates enhanced bone development in the foetal chick femur in vitro, Bone 53 (53) (2013) 468–477.

E. Schileo, F. Taddei, L. Cristofolini, M. Viceconti, Subject-specific finite element models implementing a maximum principal strain criterion are able to estimate failure risk and fracture location on human femurs tested in vitro, J. Biomech. 41 (2) (2008a) 356–367.

Z. Yosibash, D. Tal, N. Trabelsi, Predicting the yield of the proximal femur using high order finite element analysis with inhomogeneous orthotropic material properties, Philos. Trans. A Math. Phys. Eng. Sci. 368 (2010) 2707–2723.

T. A. Gruen, G. M. Mcneice, H. C. Amstutz, Modes of Failure of Cemented Stem–type Femoral Components: A Radiographic Analysis of Loosening, Clin. Orthop. Relat. Res. 141 (1979) 17–27.

E. Schileo, E. DallAra, F. Taddei, A. Malandrino, T. Schotkamp, M. Baleani, M. Viceconti, An accurate estimation of bone density improves the accuracy of subject-specific finite element models, J. Biomech. 41 (2008b) 2483–2491.

G. H. Isaac, C. A. Busch, V. Shetty, K. J. Drabu, Radiographic assessment of the cement

mantle thickness of the femoral stem in total hip replacement: a case study of 112 consecutive implants, Proc. Inst. Mech. Eng. H 214 (5) (2000) 471–477.

R. L. Jayasuriya, S. C. Buckley, A. J. Hamer, R. M. Kerry, I. Stockley, M. W. Tomouk, J. M. Wilkinson, Effect of sliding-taper compared with composite-beam cemented femoral prosthesis loading regime on proximal femoral bone remodeling: a randomized clinical trial, J. Bone. Joint. Surg. Am. 95 (1) (2013) 19–27.

M. G. Li, S. M. Rohrl, D. J. Wood, B. Nivbrant, Periprosthetic changes in bone mineral density in 5 stem designs 5 years after cemented total hip arthroplasty. No relation to stem migration, J. Arthroplasty 22 (5) (2007) 689–691.

P. K. Venesmaa, H. P. J. Kroger, J. S. Jurvelin, H. J. A. Miettinen, O. T. Suomalainen, E. M. Alhava, Periprosthetic bone loss after cemented total hip arthroplasty Periprosthetic bone loss after cemented total hip arthroplasty, Acta. Orthop. Scand. 74 (1) (2003) 31–36.

G. Digas, J. Karrholm, Five-year DEXA study of 88 hips with cemented femoral stem, Int. Orthop. 33 (6) (2008) 1495–1500.

A. J. Buckland, M. M. Dowsey, J. D. Stoney, A. J. Hardidge, K. W. Ng, P. F. M. Choong, Periprosthetic bone remodeling using a triple-taper polished cemented stem in total hip arthroplasty, J. Arthroplasty 25 (7) (2010) 1083–1090.

R. Bieger, F. Martini, H. Reichel, R. Decking, Changes of periprosthetic bone density after implantation of an anatomical femoral stem with cemented and cementless fixation, Hip Int. 21 (3) (2011) 317–24.

A. R. Knutsen, N. Lau, D. B. Longjohn, E. Ebramzadeh, S. N. Sangiorgio, Periprosthetic femoral bone loss in total hip arthroplasty: systematic analysis of the effect of stem design, Hip Int. 27 (1) (2017) 26–34.

S. Scheiner, P. Pivonka, C. Hellmich, Poromicromechanics reveals that physiological bone strains induce osteocyte-stimulating lacunar pressure, Biomech. Model. Mechanobiol. 15 (1) (2016) 9–28.

M. I. Pastrama, S. Scheiner, P. Pivonka, C. Hellmich, A mathematical multiscale model of bone remodeling, accounting for pore space-specific mechanosensation, Bone 107 (2018) 208–221.

R. Schwarzkopf, J. K. Oni, S. E. Marwin, Total hip arthroplasty periprosthetic femoral fractures: a review of classification and current treatment., Bull. Hosp. Jt. Dis. 71 (1) (2013) 68–78.

Appendix A. FFI1R validation

The FE model of FFI1R was validated by experimental observations. Strains in the experiments on bone's surface were measured by digital image correlation (DIC). Validation was performed for both intact and implanted configurations. Comparison between the FE results and the experimental observations for the intact femur are detailed in Katz and Yosibash (2020) and are presented in Figure A.7. The implanted femur was loaded in two loading configurations (7^o and 0^o), strain gauges (SG) were applied to the prosthesis prior to implantation (experimental protocol is similar to the one presented in Katz et al. (2018)). The agreement between the experimental results and the FE simulations for the implanted femur are shown in Figures A.8 and A.9.

A good agreement was obtained for both implanted and intact femur states including measurements on the prosthesis inside the femur.

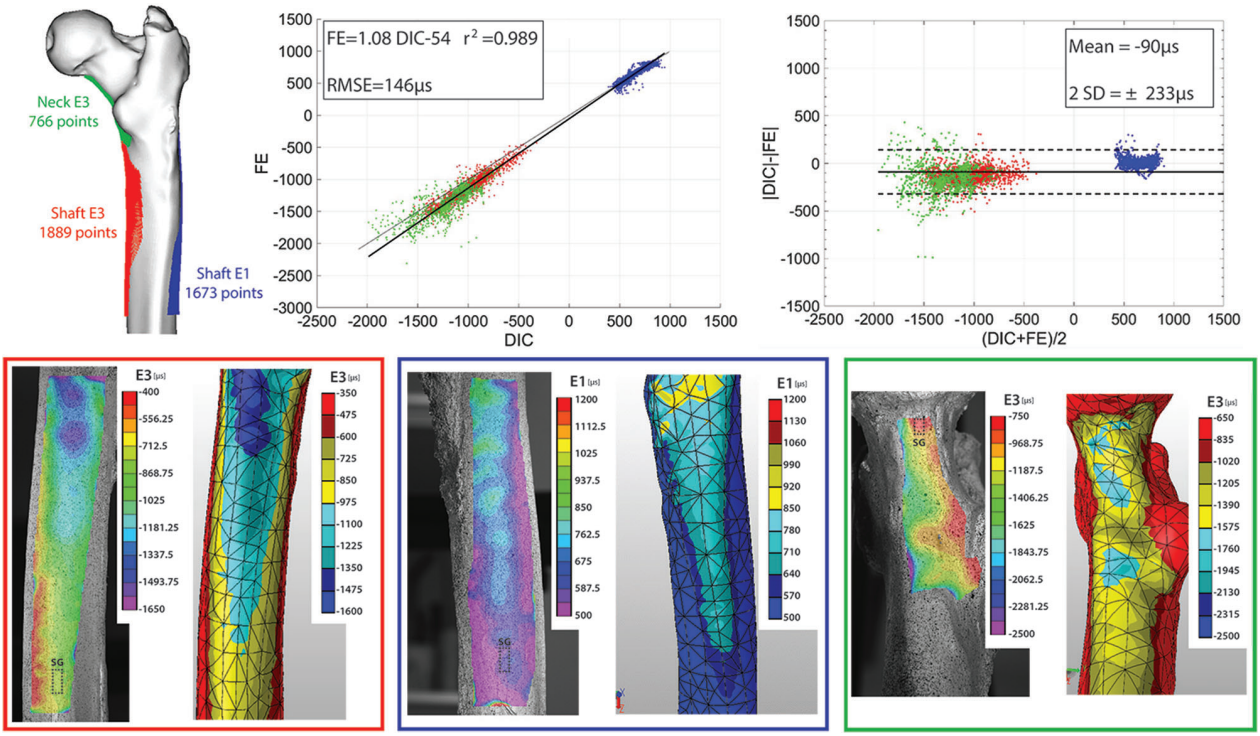

Figure A.7: Comparison of the strain fields obtained from DIC measurements to FE predictions at 7^o under 1000N loading for the intact FFI1R. Linear correlations and Bland Altman plots are presented. All units are micro-strains. **The results are taken from Katz and Yosibash (2020)**

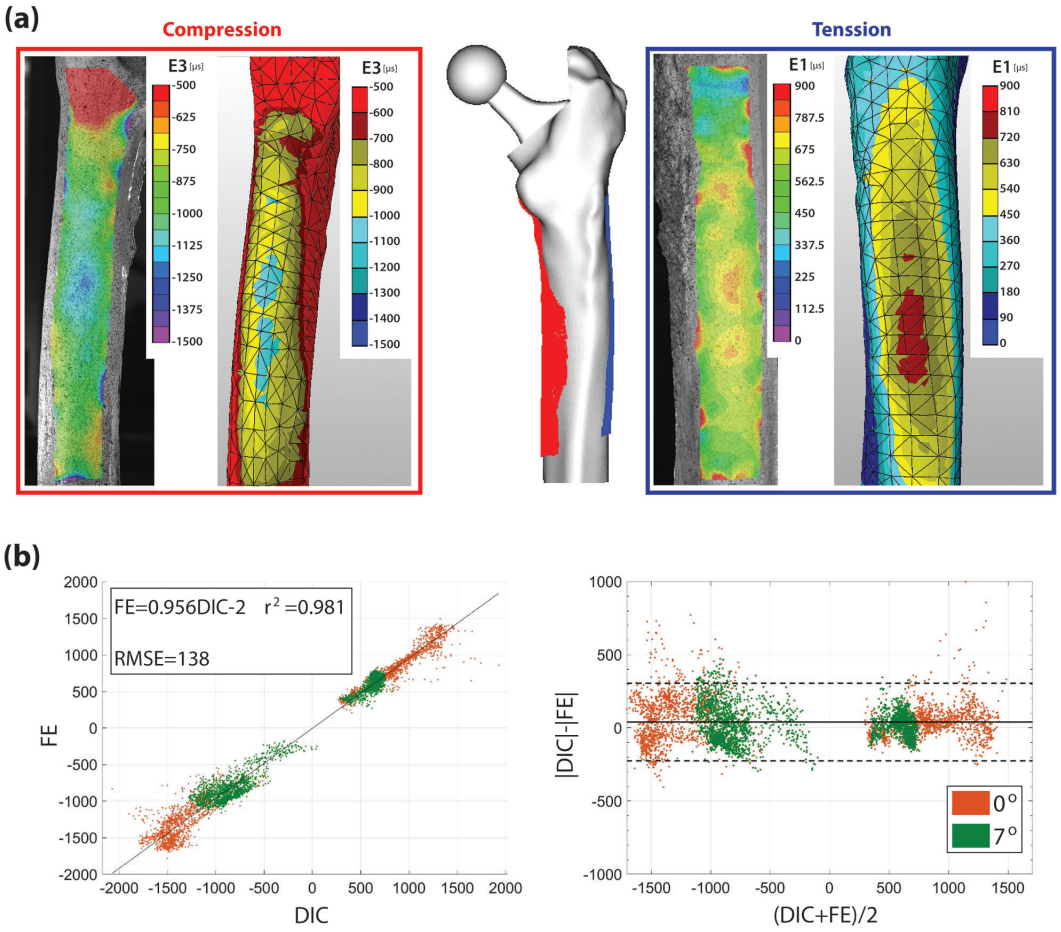

Figure A.8: Validation of the predicted surface strains for the implanted FFI1R. (a) Comparison of the strain fields obtained from DIC measurements to FE predictions at 7^o under 1000N loading. (b) Bland Altman and linear correlation plots comparing FE predictions to DIC measurements. Both 7^o and 0^o loading angles were considered under 1000N loading. All units are micro-strains.

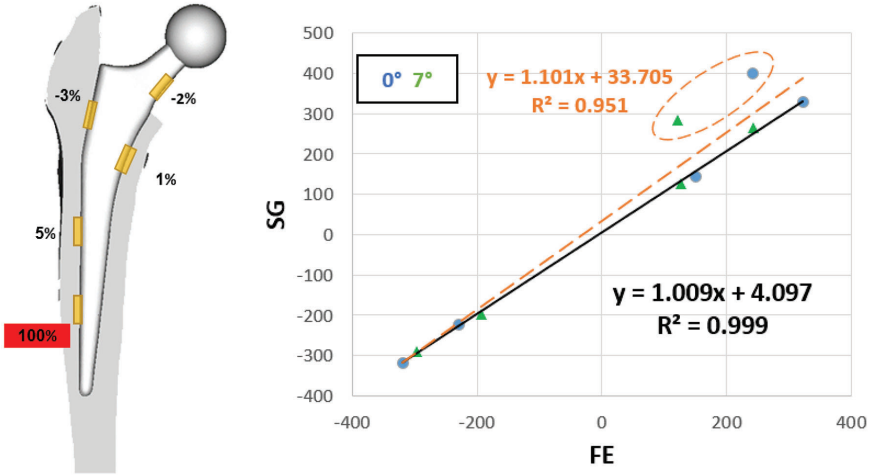

Figure A.9: Comparison of the SG measurements to FE predictions on the implants surface. Left: The SG locations on the implant surface with the average relative difference between experimental and predicted strains. Right: A linear correlation plot. Four out of the five examined SGs showed a very good agreement.